Biomedical Signal Processing and Control 5 (2010) 299–310

Contents lists available at ScienceDirect

Biomedical Signal Processing and Control

journal homepage: www.elsevier.com/locate/bspc

Analysis of heart rate variability during exercise stress testing using respiratory information

Raquel Bailón[a,b,*], Luca Mainardi[c], Michele Orini[a,b,c], Leif Sörnmo[d], Pablo Laguna[a,b]

[a] Communications Technology Group (GTC) at the Aragón Institute of Engineering Research (I3A), University of Zaragoza, María de Luna 1, 50018 Zaragoza, Spain
[b] CIBER de Bioingeniería, Biomateriales y Nanomedicina (CIBER-BBN), Spain
[c] Department of Bioengineering, Politecnico di Milano, via Golgi 39, 20133 Milano, Italy
[d] Signal Processing Group, Department of Electrical and Information Technology, Lund University, Lund, Sweden

ARTICLE INFO

Article history:
Received 8 January 2010
Received in revised form 19 April 2010
Accepted 17 May 2010
Available online 18 June 2010

Keywords:
Heart rate variability
Exercise stress testing
Respiratory frequency
Time–frequency analysis
Parametric decomposition

ABSTRACT

This paper presents a novel method for the analysis of heart rate variability (HRV) during exercise stress testing enhanced with respiratory information. The instantaneous frequency and power of the low frequency (LF) and high frequency (HF) bands of the HRV are estimated by parametric decomposition of the instantaneous autocorrelation function (ACF) as a sum of damped sinusoids. The instantaneous ACF is first windowed and filtered to reduce the cross terms. The inclusion of respiratory information is proposed at different stages of the analysis, namely, the design of the filter applied to the instantaneous ACF, the parametric decomposition, and the definition of a dynamic HF band. The performance of the method is evaluated on simulated data as well as on a stress testing database. The simulation results show that the inclusion of respiratory information reduces the estimation error of the amplitude of the HF component from 3.5% to 2.4% in mean and related SD from 3.0% to 1.7% when a tuned time smoothing window is used at an SNR of 15 dB. Results from the stress testing database show that information on respiratory frequency produces HF power estimates which closely resemble those from the simulations which exhibited lower SD. The mean SD of these estimates with respect to their mean trends is reduced by 84% (from 0.74×10^{-3} s^{-2} to 0.12×10^{-3} s^{-2}). The analysis of HRV in the stress testing database reveals a significant decrease in the power of both the LF and HF components around peak stress.

1. Introduction

Spectral analysis of heart rate variability (HRV) is widely used as a non-invasive technique for the assessment of the autonomic nervous system (ANS) activity on the heart and the balance between the sympathetic and parasympathetic systems [1]. This balance may be altered under certain pathological conditions, such as myocardial infarction, diabetic neuropathy [1], and cardiac ischemia [2,3]. Standards of measurement, physiological interpretation and clinical use of HRV in resting conditions have been established, involving three different spectral components: a very low frequency (VLF) component in the range between 0 and 0.04 Hz, a low frequency (LF) component between 0.04 and 0.15 Hz, and a high frequency (HF) component between 0.15 and 0.4 Hz [1]. The power in the HF band is considered to be a measure of parasympathetic activity, mainly due to respiratory sinus arrhythmia (RSA). The power in the LF band is considered to be a measure of sympathetic and parasympathetic activity, together with other regulatory mechanisms such as the rennin–angiotensin system and baroreflex [4], its interpretation being controversial when, e.g. the respiratory frequency lies in the LF band.

Certain indices of HRV analysis during exercise stress testing have shown added value in the diagnosis of coronary artery disease [5]. The analysis of HRV during stress testing is challenging due to the non-stationary recording conditions. The factors which influence HRV during spontaneous conditions [6] are altered during exercise [7]. Several approaches to non-stationary analysis of HRV have been proposed in the literature [8], of which time–frequency (TF) analysis is the most common. This approach can be divided into three categories: (i) non-parametric methods based on linear filtering, including the short-time Fourier transform [9–11] and the wavelet transform [12–14], (ii) non-parametric quadratic TF representations, including the Wigner–Ville distribution and its filtered versions [15–17], and (iii) parametric methods based on autoregressive models with time-varying coefficients [18,10]. The smoothed pseudo Wigner–Ville distribution (SPWVD) provides better resolution than non-parametric linear methods, independent control of time and frequency filtering, and power estimates

* Corresponding author at: Communications Technology Group (GTC) at the Aragón Institute of Engineering Research (I3A), University of Zaragoza, María de Luna 1, Ed. Ada Byron, 50018 Zaragoza, Spain.
E-mail address: rbailon@unizar.es (R. Bailón).

1746-8094/$ – see front matter © 2010 Elsevier Ltd. All rights reserved.
doi:10.1016/j.bspc.2010.05.005

with lower variance than parametric methods when rapid changes occur [16,19]. The main drawback of the SPWVD is the presence of cross terms, which can be attenuated by time and frequency filtering. In this work an approach for overcoming this drawback in the context of HRV analysis during stress testing is considered.

The coupling between the cardiovascular and respiratory systems results in modulation of the heart rate, i.e. RSA, mainly due to parasympathetic activity at rest [20–22]. However, the use of measures extracted from the RSA as indices of parasympathetic activity during exercise is questionable. During exercise, inhibition of the parasympathetic activity is followed by an increase in the sympathetic activity at high work loads [23,7]. According to the parasympathetic withdrawal, the RSA decreases from the beginning of the exercise, whereas an increase in RSA is observed during high work loads which cannot be explained by parasympathetic activity. This increase can be attributed to mechanical stretching of the sinus node in response to a ventilation increase [24,25].

The fact that respiratory frequency is not restricted to the classical HF band [0.15, 0.4] Hz during exercise stress testing makes it necessary to redefine the HF band [26]. In some studies, the HF band is extended to include the whole range of possible respiratory frequencies [27,28,9,29,13], the upper limit being half the mean heart rate (HR). In other cases, the HF band is centered on the respiratory frequency with constant or time-dependent bandwidth [14]. The LF band can be redefined to range from its lower limit (i.e. 0.04 Hz) to the lower limit of the HF band.

In this paper, a method for HRV analysis during exercise stress testing is presented which makes use of information on respiratory frequency. The objective of this work is to propose a method for HRV analysis during stress testing which makes use of information on respiratory frequency when estimating the instantaneous frequency and power of the LF and HF components. The method is an extension of the parametric decomposition of the instantaneous autocorrelation function (ACF) on which the SPWVD is based, previously applied to analysis of HRV during tilt test [17]. The method assumes that the instantaneous ACF of the HRV can be decomposed, at each time instant, as a sum of damped sinusoids from which the instantaneous frequency and power of the LF and HF components are derived. The methods are presented in Section 2, the simulation study and the exercise stress testing database in Section 3, the results in Section 4 and, finally, a discussion is found in Section 5.

2. Methods

The estimation of the instantaneous frequency and power of the HRV components is performed in three steps: (i) the computation of the windowed and filtered instantaneous ACF of the HRV analytic signal, (ii) its parametric decomposition to obtain the instantaneous amplitude and frequency of the HRV components, and (iii) the estimation of the instantaneous frequency and power of the LF and HF components. The inclusion of respiratory information will be considered for: (i) adapting the time smoothing window that filters the ACF in order to make estimation errors independent of the rate of variation of respiratory frequency, (ii) constraining the decomposition of the instantaneous ACF in order to reduce the estimation error, and (iii) dynamic definition of the HF band in order to consider respiratory frequencies that may be outside the standard HF band. The method is described by the block diagram shown in Fig. 1.

2.1. Model of heart rate variability during stress testing

Heart rate variability may be modeled as a sum of two or more sinusoids whose frequencies vary linearly in time [17]. During stress testing, the LF and HF components are represented by two sinusoids which are embedded in additive white Gaussian noise (AWGN). The analytic HRV signal $x(n)$ may be modeled as

$$x(n) = A_{\mathrm{LF}}(n)e^{j2\pi f_{\mathrm{LF}}n} + A_{\mathrm{HF}}(n)e^{j2\pi(\alpha n^2+\beta n)} + v(n). \tag{1}$$

The LF component is defined by the amplitude $A_{\mathrm{LF}}(n)$ and the discrete frequency f_{LF}, assumed to be constant during the stress test. The HF component is defined by the amplitude $A_{\mathrm{HF}}(n)$ and the instantaneous discrete frequency $f_{\mathrm{HF}}(n) = 2\alpha n + \beta$, where 2α represents the slope of $f_{\mathrm{HF}}(n)$ and β the intercept; thus, the frequency is assumed to increase linearly with work load until peak stress and then decrease linearly during recovery [25,30]. The discrete frequencies are related to the analog frequencies through the sampling rate F_s ($F_{\mathrm{LF}} = f_{\mathrm{LF}}F_s$, $F_{\mathrm{HF}} = f_{\mathrm{HF}}F_s$, respectively). The term $v(n)$ represents the analytic signal of the AWGN, which accounts for jitter in the QRS fiducial point as well as for modeling inaccuracies.

It is assumed that the variations in the LF and HF amplitudes are slow compared to the LF and HF oscillations, respectively, so that the "quasi-stationary" condition is fulfilled [31]. As a result, the model in (1) can be simplified so that, locally, $A_{\mathrm{LF}}(n) \simeq A_{\mathrm{LF}}$ and $A_{\mathrm{HF}}(n) \simeq A_{\mathrm{HF}}$.

The VLF component is not considered in this model since it cannot be estimated during stress testing.

2.2. The instantaneous autocorrelation function

The discrete SPWVD of a real-valued discrete-time signal, whose analytic version is $x(n)$, is defined by [32,33,31]

$$P_x(n,m) = 2\sum_{k=-K+1}^{K-1} |h(k)|^2 \left[\sum_{n'=-N+1}^{N-1} g(n')x(n+n'+k)x^*(n+n'-k)\right] \times e^{-j2\pi(m/M)k}; \quad m = -M+1,\ldots,M, \tag{2}$$

where n and m are the time and frequency indices, respectively. The term $g(n')$ is a symmetric time smoothing window of length $2N-1$. The term $|h(k)|^2$ is a symmetric frequency smoothing window of length $2K-1$ ($2K-1 < 2M$). In order to conserve the energy the time and frequency windows are normalized so that $\sum_{n'=-N+1}^{N-1} g(n') = 1$ and $|h(0)|^2 = 1$, respectively.

The distribution $P_x(n, m/2)$ can be viewed as the discrete Fourier transform of $r_x(n,k)$, which is the instantaneous ACF $x(n+k)x^*(n-k)$ filtered by $g(n')$ and windowed by $|h(k)|^2$,

$$r_x(n,k) = |h(k)|^2 \left[\sum_{n'=-N+1}^{N-1} g(n')x(n+n'+k)x^*(n+n'-k)\right]. \tag{3}$$

We will now derive the ACF for the model in (1). The instantaneous ACF of $x(n)$ is given by

$$x(n+k)x^*(n-k) = |A_{\mathrm{LF}}|^2 e^{j2\pi f_{\mathrm{LF}}2k} + |A_{\mathrm{HF}}|^2 e^{j2\pi f_{\mathrm{HF}}(n)2k} + 2\mathcal{R}\{A_{\mathrm{LF}}A_{\mathrm{HF}}^*\}\cos\left[2\pi(\alpha(n^2+k^2)+(\beta-f_{\mathrm{LF}})n)\right] \times e^{j2\pi(f_{\mathrm{LF}}+f_{\mathrm{HF}}(n))k} + w(n+k)w^*(n-k), \tag{4}$$

where the term $w(n+k)w^*(n-k)$ accounts for all the noise contributions, including $v(n+k)v^*(n-k)$ as well as the cross products between the signal components and the noise. Using a rectangular window for time smoothing [17]

$$g(n') = \begin{cases} \dfrac{1}{2N-1}, & n' = -N+1,\ldots,N-1 \\ 0, & \text{otherwise,} \end{cases} \tag{5}$$

and an exponential window for frequency smoothing

$$|h(k)|^2 = \begin{cases} e^{-\gamma|k|}, & k = -K+1,\ldots,K-1 \\ 0, & \text{otherwise,} \end{cases} \tag{6}$$

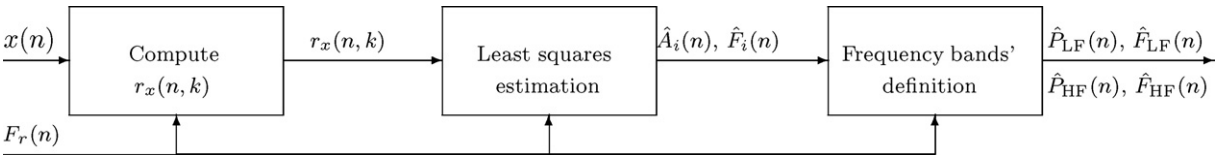

Fig. 1. Block diagram of the method for HRV analysis, where $x(n)$ stands for the analytic HRV signal, $r_x(n,k)$ is the windowed and filtered instantaneous ACF, $\hat{A}_i(n)$ and $\hat{F}_i(n)$ are the instantaneous amplitude and frequency of the HRV components, and $\hat{P}_{LF}(n)$, $\hat{F}_{LF}(n)$, $\hat{P}_{HF}(n)$ and $\hat{F}_{HF}(n)$ are the instantaneous power and frequency of the LF and HF components, respectively.

the windowed and filtered ACF $r_x(n,k)$ becomes (see Appendix A for derivation)

$$r_x(n,k) = |A_{LF}|^2 e^{-\gamma|k|} e^{j2\pi f_{LF}2k} + \frac{1}{2N-1}|A_{HF}|^2 e^{-\gamma|k|}\frac{\sin(2\pi 2\alpha(2N-1)k)}{\sin(2\pi 2\alpha k)} e^{j2\pi f_{HF}(n)2k} + \frac{1}{2N-1} 2\mathcal{R}\{A_{LF}A_{HF}^*\} e^{-\gamma|k|}\left(\sum_{n'=-N+1}^{N-1} c(n,n',k) e^{j2\pi 2\alpha n' k}\right) \times e^{j2\pi(f_{LF}+f_{HF}(n))k} + r_w(n,k). \quad (7)$$

Due to time smoothing, the amplitude and bandwidth of the HF component depend on 2α and $2N-1$ (see (7)). Note that the amplitude of the cross term can be considerably reduced by proper selection of $2N-1$. In Fig. 2, $P_x(n,m)$ is displayed for two time instants n_1 and n_2 with identical instantaneous frequency but with $2|\alpha_2| > 2|\alpha_1|$. The HF peak at n_1 is higher and narrower than the one at n_2.

2.3. Parameter estimation

The estimation of $F_{LF}(n)$, $A_{LF}(n)$, $F_{HF}(n)$, and $A_{HF}(n)$ is addressed by the parametric decomposition of $r_x(n,k)$ in (7)[17], which can be decomposed for each time instant n into a sum of complex damped sinusoids plus noise. In fact, the term related to the LF component is in itself a complex damped sinusoid, whereas the term related to the HF component can be approximated by a complex damped sinusoid provided that the damping parameter γ is large enough to attenuate the lobes of the term $\sin(2\pi 2\alpha(2N-1)k)/\sin(2\pi 2\alpha k)$; the interference term is assumed to be small, as illustrated in Fig. 2, due to the use of (5) and (6), and is included in the noise term. Note that, although the parameters F_{LF}, A_{LF} and A_{HF} have been assumed constant for the derivation of $r_x(n,k)$, their estimation is made dependent on n since they are estimated for each time instant.

The function $r_x(n,k)$ is assumed to consist of a time-varying number $I(n)$ of complex damped sinusoids corrupted by AWGN $u(n,k)$,

$$r_x(n,k) = \sum_{i=1}^{I(n)} C_i(n) e^{(-\xi_i(n)+j\omega_i(n))k} + u(n,k), \quad k = 0,1,\ldots,K-1, \quad (8)$$

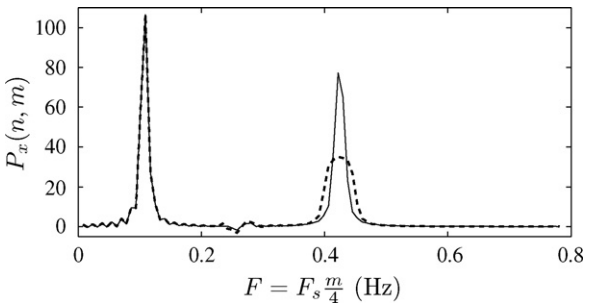

Fig. 2. The SPWVD $P_x(n,m)$ for two time instants, n_1 (solid line) corresponds to 250 s, and n_2 (dashed line) corresponds to 817 s, such as $F_{LF}(n_1) = F_{LF}(n_2) = 0.1$ Hz, $F_{HF}(n_1) = F_{HF}(n_2) = 0.42$ Hz, $2|\alpha_1|F_s = 1.67 \times 10^{-4}$ Hz/s and $2|\alpha_2|F_s = 5.00 \times 10^{-4}$ Hz/s. Note the reduced amplitude of the interference terms.

where $u(n,k)$ includes the noise term $r_v(n,k)$, the interference term (i.e., third term in (7)), and modeling inaccuracies. Once the parameters $\omega_i(n)$ and $C_i(n)$ of the $I(n)$ complex damped sinusoids are estimated, the instantaneous amplitude and frequency of LF and HF components can be derived. Note that $I(n) = 2$ for all time instants when the model in (1) is assumed. However, a time-varying number of sinusoids $I(n)$ is considered so as to account for the fact that more than two components usually exist in HRV signals. For example, a pedalling component is sometimes present in stress testing in addition to the LF and HF components [34].

The parameters $C_i(n)$, $\xi_i(n)$ and $\omega_i(n)$ are estimated using a suboptimal least-squares (LS) approach in which the properties of a prediction error filter polynomial $B_n(z) = 1 + b(n,1)z^{-1} + b(n,2)z^{-2} + \ldots + b(n,P)z^{-P}$ are explored [35]. In the absence of noise the following linear prediction equation of order P should be fulfilled,

$$\mathbf{R}_\mathbf{x}(n)\mathbf{b}(n) = -\mathbf{r}_\mathbf{x}(n), \quad (9)$$

where

$$\mathbf{R}_\mathbf{x}(n) = \begin{bmatrix} r_x^*(n,1) & r_x^*(n,2) & \ldots & r_x^*(n,P) \\ r_x^*(n,2) & r_x^*(n,3) & \ldots & r_x^*(n,P+1) \\ \vdots & \vdots & & \vdots \\ r_x^*(n,K-P) & r_x^*(n,K-P+1) & \ldots & r_x^*(n,K-1) \end{bmatrix} \quad (10)$$

$$\mathbf{b}(n) = [b(n,1)b(n,2)\ldots b(n,P)]^T,$$

$$\mathbf{r}_\mathbf{x}(n) = [r_x^*(n,0)r_x^*(n,1)\ldots r_x^*(n,K-P-1)]^T.$$

It can be shown that, in the absence of noise, $B_n(z)$ has zeros at $z_i(n) = e^{(\xi_i(n)+j\omega_i(n))}$, if P is chosen so as to satisfy $I(n) \le P \le K - I(n)$ [36].

In the presence of noisy data $\mathbf{b}(n)$ can be estimated in the LS sense by minimizing

$$J_n = (\mathbf{r}_\mathbf{x}(n) + \mathbf{R}_\mathbf{x}(n)\mathbf{b}(n))^H(\mathbf{r}_\mathbf{x}(n) + \mathbf{R}_\mathbf{x}(n)\mathbf{b}(n)), \quad (11)$$

resulting in

$$\hat{\mathbf{b}}(n) = -(\mathbf{R}_\mathbf{x}^H(n)\mathbf{R}_\mathbf{x}(n))^{-1}\mathbf{R}_\mathbf{x}^H(n)\mathbf{r}_\mathbf{x}(n). \quad (12)$$

The inaccuracies in $\hat{\mathbf{b}}(n)$ introduced by the presence of the noise $u(n,k)$ can be alleviated by substituting $\mathbf{R}_\mathbf{x}(n)$ with its truncated singular value decomposition (SVD) $\hat{\mathbf{R}}_\mathbf{x}(n)$, where the smallest singular values of $\mathbf{R}_\mathbf{x}(n)$ are set to zero [35]. In this study the singular values smaller than 10% of the largest singular value are set to zero and, accordingly, the number of complex damped sinusoids $I(n)$ can be estimated directly as the rank of $\hat{\mathbf{R}}_\mathbf{x}(n)$.

The parameters $\xi_i(n)$ and $\omega_i(n)$ can be derived from the zeros of $B_n(z)$,

$$\xi_i(n) = \mathcal{R}\{\ln(z_i(n))\}, \quad \omega_i(n) = \mathcal{I}\{\ln(z_i(n))\}, \quad (13)$$

and, after replacing their estimates in (8), the parameters $C_i(n)$ can be obtained as the LS solution of the linear system. Then, the amplitude and frequency of the complex sinusoids of $x(n)$ can be obtained

as

$$F_i(n) = \frac{1}{2}\frac{\omega_i(n)}{2\pi}F_s, \quad A_i(n) = \sqrt{|C_i(n)|}. \tag{14}$$

The LF and HF components can be chosen as the two sinusoids with highest power whose estimated frequency $\hat{F}_i(n)$ lies in the LF and HF band, respectively.

$$\hat{F}_{\mathrm{LF}}(n) = arg\max_{F_i \in \Omega_{\mathrm{LF}}} A_i(n), \quad \hat{A}_{\mathrm{LF}}(n) = \max_{F_i \in \Omega_{\mathrm{LF}}} A_i(n), \tag{15}$$

$$\hat{F}_{\mathrm{HF}}(n) = arg\max_{F_i \in \Omega_{\mathrm{HF}}} A_i(n), \quad \hat{A}_{\mathrm{HF}}(n) = \max_{F_i \in \Omega_{\mathrm{HF}}} A_i(n), \tag{16}$$

where Ω_{LF} and Ω_{HF} represent the LF and HF bands, respectively, defined in Section 2.6. The instantaneous power of the LF and HF components can be estimated as $\hat{P}_{\mathrm{LF}}(n) = \hat{A}^2_{\mathrm{LF}}(n)/2$ and $\hat{P}_{\mathrm{HF}}(n) = \hat{A}^2_{\mathrm{HF}}(n)/2$, respectively.

2.4. Inclusion of information on respiratory frequency

It is now assumed that $F_{\mathrm{HF}}(n)$ can be approximated by the respiratory frequency. Then, respiratory information can be included in the estimation of the HRV components. Suppose that the zero of the prediction error filter polynomial associated with the HF component, $z_{\mathrm{HF}}(n)$, is known (see later for details), then the estimation of $\mathbf{b}(n)$ can be solved as a constrained LS problem. Since $z_{\mathrm{HF}}(n)$ is a zero of $B_n(z)$ it holds that $B_n(z_{\mathrm{HF}}) = 1 + b(n,1)z_{\mathrm{HF}}^{-1} + b(n,2)z_{\mathrm{HF}}^{-2} + \ldots + b(n,P)z_{\mathrm{HF}}^{-P} = 0$, so the constraint can be expressed as

$$c(\mathbf{b}(n)) = \mathbf{b}^T(n)\mathbf{z}_{\mathrm{HF}}(n) + 1 = 0, \tag{17}$$

where $\mathbf{z}_{\mathrm{HF}}(n) = \left[z_{\mathrm{HF}}^{-1}(n), z_{\mathrm{HF}}^{-2}(n), \ldots, z_{\mathrm{HF}}^{-P}(n)\right]^T$. The constrained LS problem can be solved by using Lagrange multipliers; the function to be minimized is

$$J_{c,n} = J_n + \mathcal{R}\left\{c(\mathbf{b}(n))\lambda^*\right\}. \tag{18}$$

The constrained LS estimator is given by (see Appendix B for derivation)

$$\hat{\mathbf{b}}_{\mathbf{c}}(n) = \hat{\mathbf{b}}(n) - \left(\hat{\mathbf{b}}^T(n)\mathbf{z}_{\mathrm{HF}}(n) + 1\right)\left(\mathbf{z}_{\mathrm{HF}}^H(n)\left[\left(\mathbf{R}_{\mathbf{x}}^H(n)\mathbf{R}_{\mathbf{x}}(n)\right)^{-1}\right]^T\mathbf{z}_{\mathrm{HF}}(n)\right)^{-1} \times \left(\mathbf{R}_{\mathbf{x}}^H(n)\mathbf{R}_{\mathbf{x}}(n)\right)^{-1}\mathbf{z}_{\mathrm{HF}}^*(n). \tag{19}$$

In order to apply (19), knowledge of the zero $z_{\mathrm{HF}}(n) = e^{\xi_{\mathrm{HF}}(n)+j2\pi 2f_{\mathrm{HF}}(n)}$ is required which, in turn, requires knowledge of the instantaneous frequency $f_{\mathrm{HF}}(n)$, being approximated by the respiratory frequency $f_r(n)$, and the damping factor $\xi_{\mathrm{HF}}(n)$ whose estimation is described in the following. We start by recalling the HF component from (7) and (8)

$$\frac{1}{2N-1}|A_{\mathrm{HF}}|^2 e^{-\gamma|k|}\frac{\sin(2\pi 2\alpha(2N-1)k)}{\sin(2\pi 2\alpha k)}e^{j2\pi f_{\mathrm{HF}}(n)2k} \simeq C_{\mathrm{HF}}(n)e^{-\xi_{\mathrm{HF}}(n)k}e^{j\omega_{\mathrm{HF}}(n)2k}. \tag{20}$$

One approach is to approximate the envelope $(1/(2N-1))(\sin(2\pi 2\alpha(2N-1)k))/(\sin(2\pi 2\alpha k))$ by an exponential fit $e^{-\delta|k|}$. The periodicity due to the term $\sin(2\pi 2\alpha k)$ makes the approximation valid only if $2\pi 2|\alpha|k < \pi/2$, i.e. $8|\alpha|k < 1$. If $\delta|k| \ll 1$, the exponential fit can be approximated by a linear fit $e^{-\delta|k|} \simeq 1 - \delta|k|$. The fitting is performed in a window of length $1/\gamma$ where it can be assumed that $\delta|k| \ll 1$ with a proper selection of the parameter γ. Finally, the damping factor can be approximated by $\xi_{\mathrm{HF}}(n) \simeq \gamma + \delta(n)$, where δ depends on n as 2α can also depend on n. The goodness of this approximation is a function of the value of 2α, which will be compensated for later (see Section 2.5).

The respiratory information consists of frequency $f_r(n)$ and rate of variation $2\alpha(n)$, so both parameters have to be estimated. In practice, the instantaneous rate of variation is estimated by the regressive differences

$$2\hat{\alpha}(n) = \hat{f}_r(n) - \hat{f}_r(n-1), \tag{21}$$

where $\hat{f}_r(n)$ is the respiratory frequency estimate.

2.5. Time window adaptation

2.5.1. Varying length of the rectangular time window

The amplitude and bandwidth of the HF peak depend on 2α, causing estimation errors which also depend on 2α through the approximation of the damping factor described in Section 2.4. In order to reduce this dependency, a time window $g(n')$ whose length is a function of $2\alpha(n)$ is used. This is achieved by controlling the lobes' bandwidth of the envelope of the HF component in (7) by keeping the term $2\alpha(2N-1)$ constant for each n. The time-varying time window length, $2N(n)-1$, is defined as

$$2N(n) - 1 = \frac{\kappa}{2|\hat{\alpha}(n)|}, \tag{22}$$

where κ is a constant. Note that for each n a different length is obtained in which the method assumes that the rate of variation is constant (linearly varying frequencies). An upper limit is imposed on $2N(n)-1$ to avoid very long windows, obtained mostly when the respiratory frequency is almost constant, where $2\hat{\alpha}(n)$ cannot be approximated as constant in the whole window. The upper limit is defined for each n as the maximum window length centered on n in which the standard deviation of $2\hat{\alpha}(n)$ is below a threshold $\sigma^u_{2\alpha}$.

A lower limit of the window length is determined by the maximum value of 2α, imposed by the restriction $8|\alpha|k < 1$, given in Section 2.4, which for the worst case is $2N(n) - 1 > 4\kappa K$. A note of caution is warranted when the lower limit is not large enough to attenuate the cross terms. In this application a window length of approximately 9 s allows sufficient reduction of the cross terms.

2.5.2. Tuned time window

An approach to reduce the HF amplitude estimation errors is to employ a time window such that the HF term of $r_x(n,k)$ (see (A.3) in Appendix A) becomes a complex damped sinusoid itself, without the need for approximations. This is achieved by choosing a time window $g(n')$ such that,

$$\sum_{n'=-N+1}^{N-1} g(n')e^{j2\pi 2\alpha n' 2k} = e^{-\rho(n)|2\alpha||2k|}, \tag{23}$$

where $\rho(n)$ is a positive arbitrary constant.

Assuming that the time window $g(n')$ is an even function, the term on the left hand side can be viewed as the Fourier transform $G(\Omega)$ of the discrete-time signal $g(n')$,

$$\sum_{n'=-N+1}^{N-1} g(n')e^{-j\Omega n'} = G(\Omega), \tag{24}$$

evaluated at $\Omega = 2\pi 4\alpha k$. The transform $G(\Omega)$ is periodic with 2π but if we force

$$G(\Omega) = e^{-(\rho(n)/2\pi)|\Omega|}, \quad -\pi \le \Omega \le \pi, \tag{25}$$

the time window $g(n')$ can be obtained as

$$g(n') = \frac{1}{2\pi}\int_{-\pi}^{\pi} G(\Omega)e^{j\Omega n'}d\Omega = \frac{2\rho(n)}{(2\pi n')^2 + \rho^2(n)} \times (1 - e^{-(\rho(n)/2)}\cos(\pi n')). \tag{26}$$

When $\rho(n)$ is sufficiently large (i.e. ≥ 10), $G(\Omega)$ becomes zero around $\pm\pi$ and, therefore, $g(n')$ can be approximated by

$$g(n') \simeq \frac{2\rho(n)}{(2\pi n')^2 + \rho^2(n)}. \quad (27)$$

Using this window, referred to as tuned time window, $r_x(n,k)$ becomes, in a parallel way to (A.4)

$$r_x(n,k) = |A_{LF}|^2 K_{LF} e^{-\gamma|k|} e^{j2\pi f_{LF}2k} + |A_{HF}|^2 e^{-\gamma|k|} e^{-\rho(n)|2\alpha||2k|} e^{j2\pi f_{HF}(n)2k} + 2\mathcal{R}\{A_{LF}A_{HF}^*\} e^{-\gamma|k|} \left(\sum_{n'=-N+1}^{N-1} \left\{ g(n') c(n,n',k) e^{j2\pi 2\alpha n' k} \right\} \right) \times e^{j2\pi(f_{LF}+f_{HF}(n))k} + e^{-\gamma|k|} \left(\sum_{n'=-N+1}^{N-1} \left\{ g(n') w(n+n'+k) w^*(n+n'-k) \right\} \right). \quad (28)$$

where $K_{LF} = \sum_{n'=-N+1}^{N-1} g(n') = G(0) = 1$. In this case, the damping factor corresponding to the HF component is $\xi_{HF}(n) = \gamma + \rho(n)2|2\alpha|$.

Similar to the rectangular time window, the HF estimation errors can be made independent of 2α by keeping the term $\rho(n)2|2\alpha|$ constant. The parameter $\rho(n)$ is defined as,

$$\rho(n) = \frac{\eta}{2 \cdot 2|\hat{\alpha}(n)|}, \quad (29)$$

where η is a constant. An upper limit is imposed on $\rho(n)$ to avoid too large values (when the respiratory frequency is almost constant) which would mask the exponential behaviour of $G(\Omega)$. This upper limit has been empirically set to $K/2$. The lower limit of $\rho(n)$ is set to 10.

2.6. Bands' definition

In this study the LF band, Ω_{LF}, follows the standard definition [0.04, 0.15] Hz. Two approaches are considered to define the HF band, Ω_{HF}: (1) the extended HF band ranges from 0.15 Hz to half the mean HR so that it covers possible respiratory frequencies and (2) the dynamic HF band is centered on the respiratory frequency and has a bandwidth of 0.25 Hz (the lower limit of the dynamic HF band cannot fall below 0.15 Hz).

3. Materials

3.1. Simulation study

Considering that HR can reach 200 bpm during stress testing, a sampling rate of at least 3 Hz is implied. In this study a sampling rate of $F_s = 8$ Hz is used, which is above the minimum sampling rate to avoid aliasing when using the SPWVD.

In all simulations the analytic signal $x(n)$ is defined as the sum of two components: a fixed LF component at 0.1 Hz, and an HF component whose frequency varies. Two approaches have been considered to simulate the HF component:

LV (linear variation): The frequency $F_{HF}(n)$ increases and decreases linearly, mimicing the behaviour observed during exercise and recovery. A low-pass filter smooths the otherwise non-physiological transition from exercise to recovery. This simulation is included because it corresponds exactly to the model assumed in Section 2.1.

PV (physiological variation): The frequency $F_{HF}(n)$ is set to be the respiratory frequency measured during stress testing using an airflow thermistor [37]. Note that the assumption of linearly varying frequencies only needs to hold in the time interval comprised by the time window $g(n')$, usually fulfilled during stress testing.

The amplitudes $A_{LF}(n)$ and $A_{HF}(n)$ are assumed to decrease linearly from the onset of exercise to peak stress and then to increase linearly during recovery, modeling the behaviour of the sympathetic and parasympathetic activity during exercise and recovery, respectively [27,28,25]. The $A_{HF}(n)$ exhibits an increase when $F_{HF}(n)$ reaches 60% of its total increase, modeling mechanical stretching of the sinus node due to respiration [24,25]. The frequency $F_{HF}(n)$ and amplitudes $A_{LF}(n)$ and $A_{HF}(n)$ of the simulated signals are displayed in Fig. 3 for approaches LV and PV.

White Gaussian noise is added to the simulated HRV signals at a signal-to-noise ratio (SNR) defined by the ratio between the power of the LF component at the instant of maximum value (onset of the trial) and the noise variance. Different SNRs from 0 to 30 dB in 5-dB steps are considered. A total of 100 noise realizations are generated for each SNR and simulated HRV signal.

An estimate of the SNR in HRV signals during stress testing may be derived based on the literature and experimental observations. In standing position, the order of the total power of a typical HRV signal is 671 ms^2, whereas the order of the power of the LF and HF components is 308 and 95 ms^2, respectively [1]. Noise in HRV signals is mainly due to jitter in the QRS fiducial point. Assuming that the ECG signal is sampled with the rate F_{ecg}, an error of a single sample is $1/F_{ecg}$ s. This error represents a noise power of approximately 1 ms^2 for $F_{ecg} = 1000$ Hz, 4 ms^2 for $F_{ecg} = 500$ Hz and 16 ms^2 for $F_{ecg} = 250$ Hz, and a SNR of approximately 25, 19, and 13 dB, respectively.

3.2. Stress testing data

A database of standard 12-lead ECG and airflow respiratory signals, simultaneously recorded during stress testing at the University Hospital of Lund, is studied. The database contains the recordings of 14 volunteers and 20 patients referred for stress testing. The ECG is sampled at 1 kHz and the respiratory signal at 50 Hz. The stress test was performed on a bicycle ergometer whose work load increased linearly each minute. The subjects were asked to cycle at a rate of 60 rpm. A detailed description of the database is given in [37].

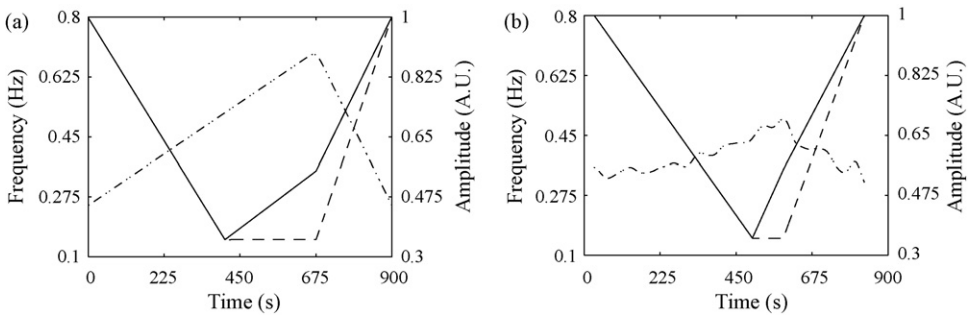

Fig. 3. The frequency $F_{HF}(n)$ (dashed-dotted line) and the amplitudes $A_{LF}(n)$ (dashed line) and $A_{HF}(n)$ (solid line), for simulations (a) LV and (b) PV.

Table 1
Parameter values.

Parameter	$2M$	$2K-1$	γ	$2N-1$		η	κ	$\sigma^u_{2\alpha}$
Value	1024	1023	1/128	81 [a]	255 [b]	0.0133	0.0084	6.6667×10^{-6}
Units	Samples	Samples	Samples^{-1}	Samples	Samples			Hz/s

[a] Length of the rectangular time window.
[b] Length of the tuned time window.

First, QRS detection is performed using ARISTOTLE[38]. Then, the instantaneous HR signal, $d_{HR}(n)$, is computed following a method based on the integral pulse frequency modulation model, which accounts for the presence of ectopic beats [39]. The HR signal is resampled at a sampling rate of $F_s = 8$ Hz. A time-varying mean HR signal $d_{HRM}(n)$ is obtained by low-pass filtering the HR signal with a cut-off frequency of 0.03 Hz. The HRV signal $d_{HRV}(n)$ results from $d_{HRV}(n) = d_{HR}(n) - d_{HRM}(n)$. The HRV signal $d_{HRV}(n)$ is low-pass filtered with a cut-off frequency of 0.9 Hz since a spurious 1-Hz component is sometimes observed [26], being synchronous to pedalling at 60 rpm but most likely unrelated to parasympathetic activity [34,40]. The respiratory frequency does not exceed 0.9 Hz in any of the recordings of the database.

The respiratory frequency is estimated from the airflow signal by spectral analysis [37]. The estimated respiratory frequency series $\hat{F}_r(n)$ is resampled at 8 Hz and low-pass filtered with a cut-off frequency of 0.01 Hz to avoid non-physiological abrupt variations due to estimation errors.

Four subjects were excluded from the study because $d_{HR}(n)$ contained too many artifacts or ectopic beats to obtain a reliable estimation of the HRV signal based on a criterion adapted from [39], and one subject was excluded because of unattached electrodes.

4. Results

4.1. Simulation study

The following methods are applied to the simulated HRV signals:

UCR: *U* nconstrained LS estimation using a *C* onstant length *R* ectangular time window.

CVR: *C* onstrained LS estimation using a $(2N(n)-1)$-*V* arying length *R* ectangular time window.

CVT: *C* onstrained LS estimation using a *T* uned time window with *V* arying factor $\rho(n)$.

Parameter values used are given in Table 1.

The estimated number of damped sinusoids, $\hat{I}(n)$, is 2 during the majority of the time for methods UCR, CVR and CVT and all model orders considered, even for a SNR as low as 5 dB, due to the SVD truncation of $\mathbf{R}_{\mathbf{x}}(n)$.

The mean and standard deviation (SD) of the estimation errors (in absolute value) are calculated for $\hat{A}_{LF}(n)$, $\hat{F}_{LF}(n)$, $\hat{A}_{HF}(n)$, and $\hat{F}_{HF}(n)$, averaging 100 realizations for each SNR.

For all methods, $\hat{F}_{LF}(n)$ and $\hat{F}_{HF}(n)$ were associated with errors lower than 0.002 ± 0.004 Hz (mean $\pm$ SD) even for an SNR as low as 15 dB and a model order as low as $P = 8$. The inclusion of informa-

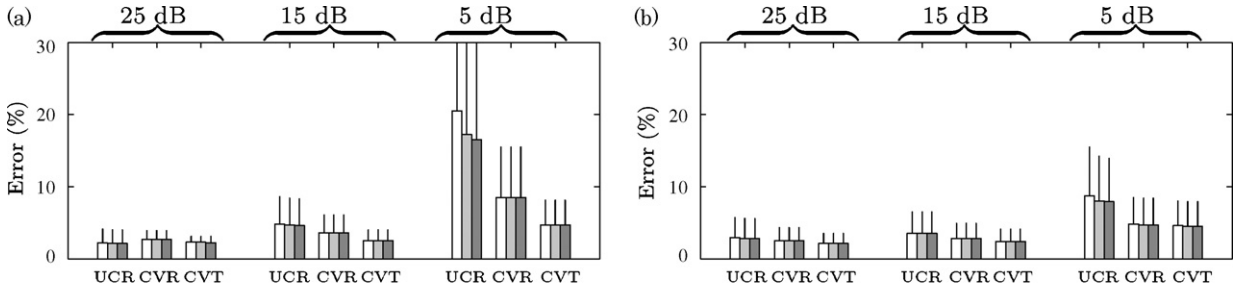

	p	25 dB	15 dB	5 dB
UCR	8	2.2±1.9	4.8 ±3.8	20.5±19.1
	12	2.1±1.9	4.6±3.7	16.5±13.9
	16	1.8±1.7	4.6±3.7	15.7±13.1
CVR	8	2.7±1.2	3.6±2.5	8.5±7.0
	12	2.7±1.2	3.6±2.5	8.5±7.0
	16	2.7±1.2	3.6±2.5	8.4±6.9
CVT	8	2.3±0.8	2.5±1.5	4.7±3.4
	12	2.2±0.9	2.5±1.5	4.7±3.4
	16	2.2±0.9	2.5±1.5	4.7±3.4

	p	25 dB	15 dB	5 dB
UCR	8	2.9±2.8	3.5±3.0	8.6±6.8
	12	2.8±2.7	3.5±3.0	7.9±6.0
	16	2.8±2.7	3.5±3.0	7.9±6.1
CVR	8	2.5±1.8	2.8±2.1	4.8±3.7
	12	2.5±1.8	2.8±2.1	4.7±3.7
	16	2.5±1.8	2.8±2.1	4.7±3.7
CVT	8	2.1±1.4	2.4±1.7	4.6±3.4
	12	2.1±1.4	2.4±1.7	4.5±3.4
	16	2.1±1.4	2.4±1.7	4.5±3.4

Fig. 4. Mean $\pm$ SD of the estimation error of $A_{HF}(n)$ in relative units (%) achieved by methods UCR, CVR and CVT in simulations (a) LV and (b) PV. Results are shown for $P = 8, 12, 16$ (white, gray, dark gray) and SNR of 5, 15, and 25 dB. Numerical values are given for $P = 8, 12, 16$.

Table 2
Results of the t-test applied to estimates $\hat{A}_{HF}(n)$ obtained by methods UCR, CVR and CVT. $T_{\%}$ and $\bar{p}$ stand for the percentage of time during which $p < 0.05$ and the mean p-value during that time, respectively, for simulation PV.

P	$T_{\%}$ ($\bar{p}$)		
	UCR–CVR	UCR–CVT	CVR–CVT
(a) 25 dB			
8	95 (6×10^{-4})	96 (5×10^{-4})	97 (2×10^{-4})
12	93 (6×10^{-4})	97 (3×10^{-4})	97 (3×10^{-4})
16	92 (7×10^{-4})	97 (3×10^{-4})	98 (2×10^{-4})
(b) 15 dB			
8	85 (2×10^{-3})	83 (2×10^{-3})	94 (7×10^{-4})
12	83 (2×10^{-3})	86 (1×10^{-3})	94 (7×10^{-4})
16	80 (3×10^{-3})	89 (1×10^{-3})	94 (7×10^{-4})
(c) 5 dB			
8	66 (5×10^{-3})	56 (6×10^{-3})	80 (3×10^{-3})
12	72 (5×10^{-3})	48 (7×10^{-3})	79 (3×10^{-3})
16	64 (5×10^{-3})	41 (9×10^{-3})	79 (3×10^{-3})

tion on respiratory frequency mainly affects $\hat{A}_{HF}(n)$. Fig. 4 presents the estimation error of $A_{HF}(n)$ for the simulations LV and PV.

For simulation LV, Fig. 4(a) shows that the inclusion of respiratory information leads to a reduction of the estimation error of $A_{HF}(n)$ at low SNRs, i.e., 15 and 5 dB, the smallest errors being achieved when the tuned window is used. A reduction in SD is achieved at the expense of a slight increase in mean for SNR of 25 dB. It is obvious from Fig. 4(a) that the estimation error does not depend on P when respiratory information is included.

For simulation PV, Fig. 4(b) shows that respiratory information again leads to a reduction of the estimation error of $A_{HF}(n)$ for all values of SNR and P. It is noted that the estimation errors are smaller than those obtained in simulation LV. It is also noted that the differences in estimation error between simulations LV and PV are the smallest for CVT.

In order to test if estimates $\hat{A}_{HF}(n)$ obtained by methods UCR, CVR and CVT are statistically significant, a two-sample t-test is applied to each of the 3 possible pairwise comparisons for each time instant n. The percentage of the total time, $T_{\%}$, during which estimates $\hat{A}_{HF}(n)$, are statistically significant (p-value<0.05) is displayed in Table 2, as well as the mean p-value during that time, $\bar{p}$, for simulation PV. It can be observed that estimates $\hat{A}_{HF}(n)$ obtained by UCR, CVR and CVT are significantly different from each other during most of the time and with a small mean p-value ($T_{\%} \geq 92\%$ and $\bar{p} \leq 7 \times 10^{-4}$ for all model orders) for a SNR of 25 dB. For lower SNRs, lower values of $T_{\%}$ as well as higher values of $\bar{p}$ are observed, mainly due to the increase in the SD of the estimates. However estimates $\hat{A}_{HF}(n)$ obtained by CVR and CVT are significantly different during at least 80% of the total time ($\bar{p} \leq 3 \times 10^{-3}$) even for a SNR of 5 dB.

The estimation error of $\hat{A}_{LF}(n)$ is similar to that of $\hat{A}_{HF}(n)$ when respiratory information is not included in the estimation of $\hat{A}_{HF}(n)$ (results not displayed), always that the model order is high enough.

Fig. 5 displays the simulated signal and the corresponding estimates $\hat{F}_{LF}(n)$, $\hat{F}_{HF}(n)$, $\hat{A}_{LF}(n)$, and $\hat{A}_{HF}(n)$, obtained by CVT for simulation PV.

4.2. Stress testing data

The methods UCR and CVT are applied to the stress testing HRV signals, using parameter values identical to those in the simulations, see Table 1. The standard HF band and the extended HF band are used with UCR because no respiratory information is included, whereas the dynamic HF band is used with CVT.

The signals $d_{HR}(n)$ and $d_{HRV}(n)$ are displayed in Fig. 6(a) and (b), respectively, for a volunteer of the present database. The non-stationary nature of $d_{HR}(n)$ can be appreciated not only in its trend, which increases approximately linearly from onset to peak stress and decreases abruptly during recovery, but also in $d_{HRV}(n)$ with its progressive diminution of HRV from onset to peak stress and then its abrupt increase during recovery. The corresponding $P_x(n, m)$ is computed using UCR and CVT and displayed in Fig. 6(c) and (d), respectively.

Fig. 7 displays the corresponding $\hat{F}_{LF}(n)$, $\hat{P}_{LF}(n)$, $\hat{F}_{HF}(n)$, and $\hat{P}_{HF}(n)$ obtained with UCR, using either the standard or the extended HF band, and CVT, using the dynamic HF band.

For stress testing data, a lower value of P is preferred than for simulated data so as to obtain smoother estimates when the LF and HF bands do not exhibit a dominant peak. Due to the SVD truncation of $\mathbf{R_x}(n)$, the estimated number of damped sinusoids $\hat{I}(n)$ equals 1 approximately 80% of the time, and 2 the 20% left. However, if a less restrictive SVD truncation is considered, the $\hat{I}(n)$ increases significantly even for low model orders, making it difficult the identification of the LF and HF components. Note that when the respiratory frequency exceeds 0.4 Hz from about 400 to 700 s, the standard HF band leads to misestimation of the HF component (see Fig. 7(a)). This problem is avoided when either UCR, using the extended HF band (Fig. 7(b)), or CVT, using the dynamic HF band (Fig. 7(c)), is employed. In that case CVT leads to smoother estimates $\hat{P}_{HF}(n)$ than does UCR. In order to quantify the smoothness of the estimate $\hat{P}_{HF}(n)$, the SD around a mean trend, obtained by low-pass filtering of $\hat{P}_{HF}(n)$ with a cut-off frequency of 0.01 Hz, is computed. This value is averaged among the 30 recordings of the

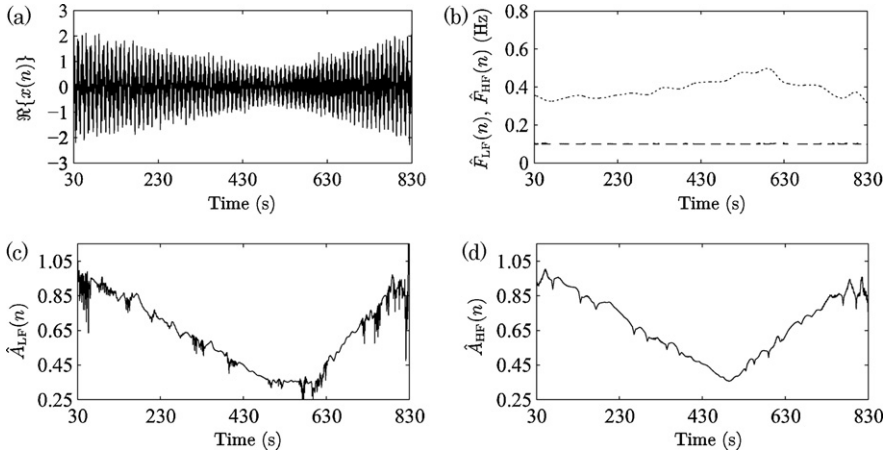

Fig. 5. (a) Simulated HRV signal $\mathcal{R}\{x(n)\}$, (b) $\hat{F}_{LF}(n)$ (dashed line) and $\hat{F}_{HF}(n)$ (dotted line), (c) $\hat{A}_{LF}(n)$, and (d) $\hat{A}_{HF}(n)$, estimated using method CVT, for a model order $P = 16$ and a SNR of 15 dB. See Fig. 3 for original trends.

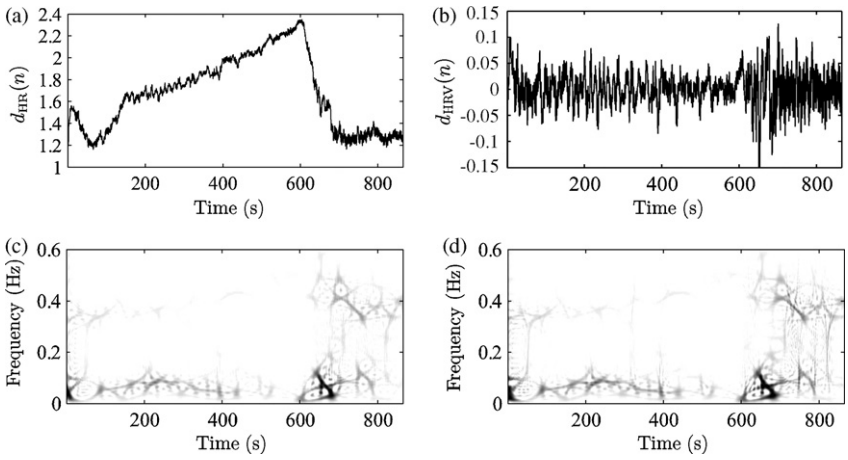

Fig. 6. (a) Instantaneous HR signal $d_{HR}(n)$, (b) HRV signal $d_{HRV}(n)$, and the SPWVD $P_x(n, m)$ using methods (c) UCR and (d) CVT for a volunteer from the database of Section 3.2.

database, yielding a mean ± SD of $0.74 \times 10^{-3} \pm 1.03 \times 10^{-3}$ s^{-2} for UCR and of $0.12 \times 10^{-3} \pm 0.18 \times 10^{-3}$ s^{-2} for CVT.

Fig. 7(b) shows trends which are similar to those in Fig. 7(c). The $\hat{F}_{LF}(n)$ varies slightly around 0.08 Hz during the whole test, while the $\hat{F}_{HF}(n)$ increases from onset to peak stress and decreases during recovery. The trend $\hat{P}_{LF}(n)$ shows a rapid decrease at the beginning of exercise, reaching a plateau which is maintained until approximately 100 s before the peak stress, when $\hat{P}_{LF}(n)$ is almost suppressed. During recovery, the initial abrupt increase in $\hat{P}_{LF}(n)$ is followed by a progressive return to the value at the beginning of the exercise. The $\hat{P}_{HF}(n)$ is decreased from onset to peak stress, but $\hat{P}_{HF}(n)$ is not suppressed around the peak stress. During the recovery there is an increase in $\hat{P}_{HF}(n)$, less steep than in $\hat{P}_{LF}(n)$, before returning to its value at the beginning of the exercise.

To test the hypothesis that the differences between $\hat{P}_{HF}(n)$ obtained by UCR (with the extended HF band) and CVT are statistically significant, a one-sample t-test is applied for each time instant n to the 14 volunteers of the database. The percentage of the total time during which differences are statistically significant (p-value <0.05) is $T_{\%} = 25\%$, and the mean p-value during that time is $\bar{p} = 0.01$. Since statistical significance is highly affected by the number of realizations (14 in this case), and to make statistical results comparable to those in the simulation study (100 realizations), the t-test is also applied to a total of 98 realizations, obtained by replicating results from the 14 volunteers, yielding statistical values of $T_{\%} = 66\%$ and $\bar{p} = 0.005$.

Fig. 8 displays the mean ± SD of the parameters $\hat{F}_{LF}(n)$, $\hat{P}_{LF}(n)$, $\hat{F}_{HF}(n)$, and $\hat{P}_{HF}(n)$, estimated using CVT and evaluated at different time instants during the stress test and averaged for the 14 volunteers. The time instants considered are: the first minute of exercise (n_1), 3 min before the peak stress (n_2), 1 min before the peak stress (n_3), 1 min after the peak stress (n_4) and 3 min after the peak stress (n_5). At each time instant, the parameter value is obtained by averaging the trend in a 1-s window.

Fig. 8 demonstrates that the over-all characteristics of the HRV trends of the 14 volunteers resemble those observed for the volunteer of Fig. 7. However, a large variability among subjects is observed in $\hat{P}_{LF}(n)$ and $\hat{P}_{HF}(n)$, especially at n_5, which may reflect the large intersubject variability that exists in HRV signals [4], especially during the recovery. To test the hypothesis that the dif-

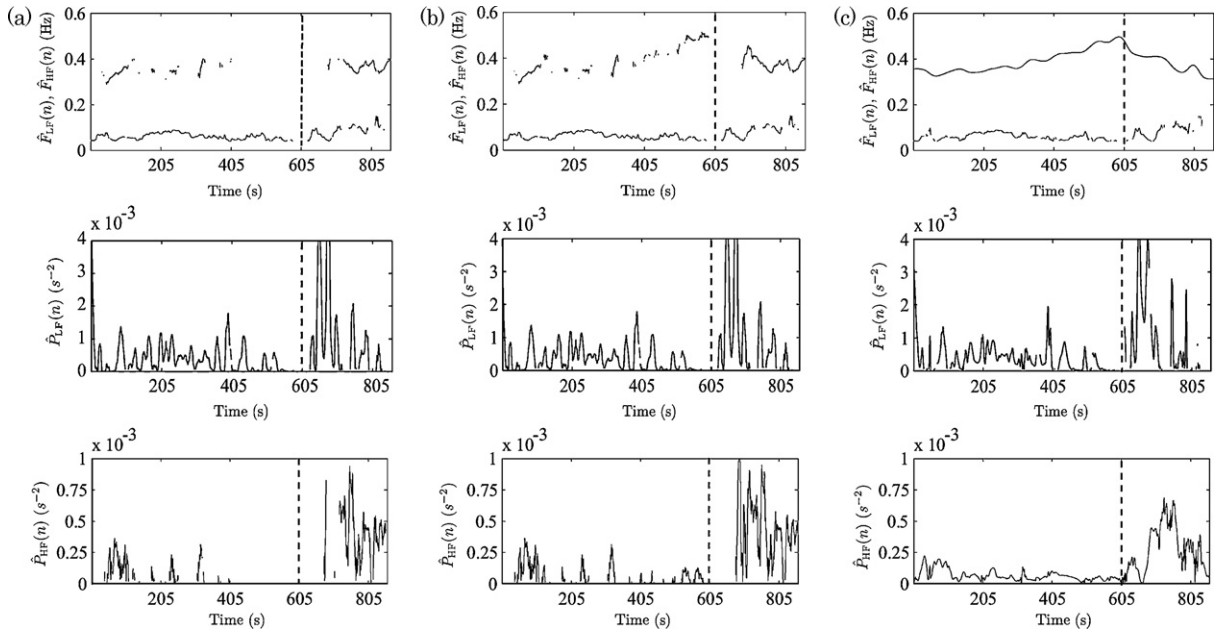

Fig. 7. The frequency trends $\hat{F}_{LF}(n)$ and $\hat{F}_{HF}(n)$ (top), $\hat{P}_{LF}(n)$ (middle), and $\hat{P}_{HF}(n)$ (bottom), using (a) UCR and standard HF band, (b) UCR and extended HF band, and (c) CVT and dynamic HF band. The model order is $P = 8$. Stress peak is marked with a dashed line.

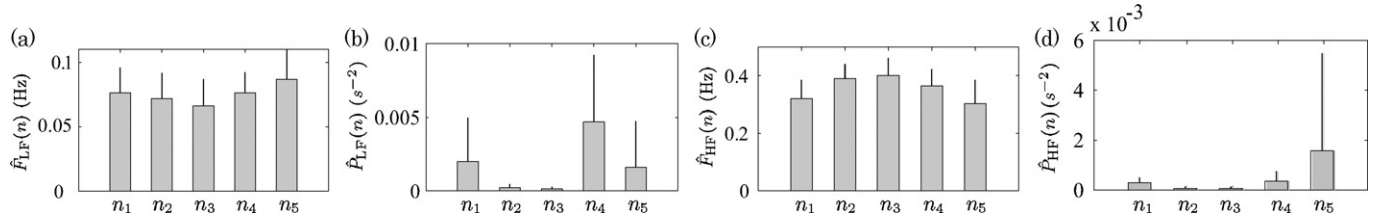

Fig. 8. Mean ± SD among the 14 volunteers of the parameters (a) $\hat{F}_{LF}(n)$, (b) $\hat{P}_{LF}(n)$, (c) $\hat{F}_{HF}(n)$, and (d) $\hat{P}_{HF}(n)$, estimated by CVT and evaluated at n_1 (the first minute of exercise), n_2 (3 min before the peak stress), n_3 (1 min before the peak stress), n_4 (1 min after the peak stress), and n_5 (3 min after the peak stress).

Table 3
The p-value obtained by the Wilcoxon signed rank test. The time instants are n_1 (the first minute of exercise), n_2 (3 min before the peak stress), n_3 (1 min before the peak stress), n_4 (1 min after the peak stress) and n_5 (3 min after the peak stress).

$\hat{F}_{HF}(n)$	n_2	n_3	n_4	n_5
n_1	0.0023	0.0017	0.0012	0.3910
n_2	–	0.1938	0.1937	0.0052
n_3	–	–	0.0203	0.0052
n_4	–	–	–	0.0040
$\hat{P}_{LF}(n)$	n_2	n_3	n_4	n_5
n_1	0.0007	0.0024	0.1189	0.4548
n_2	–	0.1016	0.0007	0.1763
n_3	–	–	0.0005	0.0137
n_4	–	–	–	0.0171
$\hat{P}_{HF}(n)$	n_2	n_3	n_4	n_5
n_1	0.0001	0.0001	*	0.0580
n_2	–	0.9515	0.0012	0.0012
n_3	–	–	0.0031	0.0009
n_4	–	–	–	0.1937

* $p > 0.05$.

ferences of HRV parameters between two time instants has zero median, a Wilcoxon signed rank test is applied to the 10 possible pair-wise comparisons of the 5 different time instants for each parameter ($\hat{F}_{LF}(n)$, $\hat{P}_{LF}(n)$, $\hat{F}_{HF}(n)$, and $\hat{P}_{HF}(n)$). The significance level (p-value) at which the null hypothesis of differences with zero median can be rejected is displayed in Tab. 3. Results are not shown for $\hat{F}_{LF}(n)$ since only the comparison $\hat{F}_{LF}(n_3) - \hat{F}_{LF}(n_5)$ obtained a significant p-value of 0.0137.

5. Discussion

5.1. Methodological aspects

In this paper the analysis of non-stationary HRV signals during stress testing is addressed by parametric decomposition of the windowed and filtered instantaneous ACF on which the SPWVD is based. The advantage of using a parametric decomposition of the instantaneous ACF is that information such as respiratory frequency can be included in the model. Respiratory information is not necessarily obtained from a simultaneously recorded respiration signal but can also be derived from the ECG signal using, e.g., the method described in [37], which has been shown to provide reliable respiratory frequency estimates during stress testing (with a mean error of 0.022 ± 0.016 Hz in a database of 29 subjects). The inclusion of respiratory information mainly affects the estimation of the amplitude of the HF component.

The inclusion of respiratory information in the definition of the time window makes estimation errors independent of the rate of variation of the respiratory frequency. This leads to shorter averaging for higher rates of variation, which results in less reduction of the cross terms and the noise. As a consequence, in benefit of the tracking of faster variations, estimation errors may be larger in the presence of high levels of noise.

The inclusion of respiratory frequency information as a constraint in the LS estimation leads to a reduction in both the mean and SD of the estimation error of the HF amplitude. This reduction depends on the time window used and on the SNR, and turns out to be larger when the tuned window is used or when lower SNRs are analyzed. For example, when the frequency of the HF component follows a real respiratory frequency, a reduction in mean from 3.5% to 2.4%, and in SD from 3.0% to 1.7%, is achieved using the tuned window for a SNR of 15 dB. For a real respiratory frequency similar results were obtained for both the tuned and the rectangular window. Estimation errors for a linearly varying HF frequency are, in general, larger than for a real respiratory frequency, and the reduction in the estimation error using a tuned window instead of a rectangular window is more evident for a linearly varying HF frequency than for a real respiratory frequency. These results may be due to the fact that the rate of variation is slower for the simulation with a real respiratory frequency. Estimation errors obtained with the tuned window are similar for both situations, thus pointing to another advantage of the tuned window. Results from the stress testing database show that the inclusion of respiratory information as a constraint in the LS estimation (using the tuned window) leads to smoother trends of the power of the HF component.

The inclusion of respiratory information in the HF band definition accounts for the fact that respiratory frequency is not restricted to the standard HF band during stress testing. In Fig. 7, it is shown that the use of the standard HF band would have yielded a misestimation of the HF component, which incorrectly can be interpreted as a suppression of the parasympathetic activity. If respiratory information is not available, this can be avoided using an extended HF band [0.15, $d_{HRM}(n)/2$] Hz [9,13]. In that case, care should be taken since other HF components unrelated to the parasympathetic activity can be merged with the respiration-related HF component (e.g. a component synchronous with the pedalling frequency [26]).

A proper selection of the time and frequency windows of the SPWVD should guarantee the reduction of the interference terms, and the decomposition of the windowed and filtered ACF as a sum of complex damped sinusoids. In this paper, an exponential window is used for frequency smoothing, and either a rectangular or a tuned window for time smoothing; other types of windows have been proposed for the analysis of HRV [15,16]. A prospective study on a larger database would be needed to obtain the most suitable values for the parameters. An alternative to reduce the interference terms could have been filtering the signal in the LF and HF bands and applying the proposed method in each band to estimate the LF and HF components separately. However, this would have required proper cut-off frequencies selection, with a particular risk when the LF and HF bands are time-varying.

It is assumed that the HRV signal during stress testing can be modeled as a sum of two sinusoids for which the frequency of the HF component varies linearly over time. While the assumption of a linearly varying HF frequency may seem drastic, it only needs to hold in the interval extended by the time window. The frequency

of the LF component can also vary during stress testing, however, its variation is much smaller than that of the HF component and it is therefore assumed to be constant. Even if the amplitudes of the LF and HF components can vary during stress testing, in the derivation of the windowed and filtered ACF they are assumed to be constant in the interval extended by the time window, given that their variations are assumed to be slow compared with the LF and HF frequencies so that the "quasi-stationary" condition is fulfilled [31]. Although the simulated signals generated to assess the performance of the method deviate from the assumed model in the sense that they include time-varying amplitudes for the LF and HF components and an HF frequency which follows a real respiratory frequency evolution during stress testing (no linearly varying as in the model), the simulated HRV signals are not able to represent the pseudo-stochastic nature of HRV signals, nor the nonlinear dynamics which may be involved in the regulation of the ANS on the heart [4]. An improved generator of synthetic HRV signals is needed to assess the performance of the method in real-life stress testing HRV signals [19]. Even with such synthetic HRV signals available, the evaluation on real stress testing HRV signals will still be of limited value as no reference "true" signal exists.

Assuming the same model for the HRV signal during stress testing, alternative approaches such as maximum likelihood estimation or noise subspace methods can be considered. The main limitation of these methods is that they assume the stationarity of the signal, in contrast to TF methods, so they need to be applied in short time windows in which the signal can be considered stationary. Different methods for the analysis of non-stationary HRV signals have been proposed in the literature. In [8] an extensive overview of methods for the continuous quantification of the LF and HF components in non-stationary HRV signals is presented, where advantages and limitations of the different approaches are highlighted. A comparison between the methods is unfortunately not straightforward, since different approaches to TF representation and HRV parameter estimation can be taken. For example, time-varying autoregressive analysis comes with the selection of estimation method for the time-varying coefficients and model order. Although spectral decomposition can be used for frequency and power estimation of the spectral components, a criterion is needed for the identification and tracking of the LF and HF components. Time-varying autoregressive analysis offers accurate frequency estimation but less accurate power estimation, especially when rapid changes occur [16,19] and when poles are close to the unit circle [8] as may be the case during stress testing. Wavelet analysis has also been used for the analysis of non-stationary HRV signals, however, as pointed out in [8], power computation may be problematic when scales and bands do not properly match or when more than one spectral component is present at a given scale, which may be the case during stress testing when respiratory frequency exhibits a large variation or when the component synchronous with the pedaling frequency is present [26]. The instantaneous power of the LF and HF components could have been alternatively estimated by integration of the SPWVD in the LF and HF bands, respectively. However, these estimates are affected by the time and frequency smoothing windows, whose effect is diminished by the parametric decomposition described in this paper, which also allows the inclusion of respiratory frequency information. The method described in this paper has been selected based on the appropriate TF resolution of the SPWVD and, especially, on the possibility of including respiration information, as proposed in this paper.

5.2. Physiological aspects

From analysis of the stress testing database (see Figs. 7 and 8) a progressive reduction of the LF power can be observed as the stress level increases, when the sympathetic activity is thought to increase also, becoming nearly abolished when peak stress is reached [27,28,41]. This would suggest either that the LF power is not a valid marker of the sympathetic activity, at least during exercise [42,43,29,4], or that some kind of saturation prevents the LF power to increase at the rate of the sympathetic stimulation. In the recovery phase there is an abrupt increase in the LF power which may be due to sympathetic activity or a rapid decrease in HR, which leaks in the LF band. The HF power is also reduced from the beginning of the exercise, which might reflect withdrawal of parasympathetic activity [27,28,4], which would allow the HR to increase and satisfy the increasing metabolic demand. While some consider HF power as a valid marker of parasympathetic activity during exercise [29], it is not always suppressed near peak stress when the parasympathetic activity is inhibited. This suggests the existence of a non-neural mechanism which causes mechanical stretching of the sinus node due to respiration [24,25]. However, in the recordings analyzed in Figs. 7 and 8, this effect is not so evident. The reason may be that the recordings come from volunteers, who perform a submaximal exercise stress test (up to a rate of perceived exertion (RPE) of 15 out of 20 on the Borg scale) [37]. Finally, the HF power increases in the recovery phase when the parasympathetic activity is supposed to be reestablished. In Figs. 7 and 8, it can be appreciated that the values of the LF and HF powers are different at the beginning and at the end of the stress testing. This might be due to the different body position at the beginning (sitting, sympathetic dominance) and at the end of the test (lying, parasympathetic dominance).

A hypothesis of this work is that the frequency of the HF component coincides with respiratory frequency. However, a reduction in the spectral coherence between the HRV and the respiration signal in the HF band in the last part of the exercise has been reported [44]. The coherence information may be also included in the HRV parameter estimation in a further study.

Finally, an important point to be discussed in the framework of this study is the use of the HRV analysis as a tool to assess changes in ANS during stress testing. It is generally accepted that HRV can be considered as a noninvasive measure of the ANS activity in stationary conditions [1]. The underlying assumption is that mean heart rate and respiratory frequency and air flow volume are stationary. During stress testing both the respiratory frequency and the air flow volume vary, yielding variations in the HF power which may be unrelated to the parasympathetic activity. Moreover, during stress testing the time-varying mean heart rate may obscure the interpretation of the evolution of the sympathetic and parasympathetic activity based on the LF and HF power estimates.

6. Conclusions

In this paper a novel method for the time-varying analysis of HRV during exercise stress testing including information on respiratory frequency has been presented. Respiratory information has been included in different parts of the analysis: in the definition of a dynamic HF band centered on the respiratory frequency, in the design of the time window based on the rate of variation of the respiratory frequency, and in the parametric decomposition as a constraint. Results from both the simulation study and the stress testing database show that the inclusion of respiratory information provides more robust estimates of the HF component in terms of mean errors and SD. The application of this technique to the stress testing database evidences a significant decrease in the power of both the LF and HF components in the vicinity of peak stress with respect to both the beginning of the exercise and the recovery. This technique can be employed to assess the, still debated, relationships between ANS control and exercise stress.

Acknowledgements

This study was supported by Ministerio de Ciencia y Tecnología, Spain, under Project TEC2007-68076-C02-02/TCM, in part by the Diputación General de Aragón (DGA), Spain, through Grupos Consolidados GTC ref:T30, by ISCIII, Spain, through CIBER CB06/01/0062, and by CAI, Spain, through Programa Europa XXI.

Appendix A.

Derivation of the windowed and filtered ACF in (3) when the rectangular window $g(n')$ in (5) is used for time smoothing and the exponential window $|h(k)|^2$ in (6) is used for frequency smoothing:

$$\begin{aligned} r_x(n,k) &= |h(k)|^2 \left[\sum_{n'=-N+1}^{N-1} g(n')x(n+n'+k)x^*(n+n'+k) \right] \\ &= e^{-\gamma|k|} \frac{1}{2N-1} \sum_{n'=-N+1}^{N-1} \left(|A_{\mathrm{LF}}|^2 e^{j2\pi f_{\mathrm{LF}}2k} + |A_{\mathrm{HF}}|^2 e^{j2\pi(2\alpha(n+n')+\beta)2k} \right. \\ &\quad + 2\mathcal{R}\{A_{\mathrm{LF}}A_{\mathrm{HF}}^*\} c(n,n',k)\, e^{j2\pi(f_{\mathrm{LF}}+2\alpha(n+n')+\beta)k} \\ &\quad \left. + w(n+n'+k)w^*(n+n'-k) \right), \end{aligned} \tag{A.1}$$

where

$$c(n,n',k) = \cos[2\pi\{\alpha[(n+n')^2+k^2] + (\beta - f_{\mathrm{LF}})(n+n')\}]. \tag{A.2}$$

Eq. (A.1) becomes

$$\begin{aligned} r_x(n,k) &= |A_{\mathrm{LF}}|^2 e^{-\gamma|k|} e^{j2\pi f_{\mathrm{LF}}2k} + \frac{1}{2N-1} |A_{\mathrm{HF}}|^2 e^{-\gamma|k|} \left(\sum_{n'=-N+1}^{N-1} e^{j2\pi 2\alpha n' 2k} \right) e^{j2\pi(2\alpha n+\beta)2k} \\ &\quad + \frac{1}{2N-1} 2\mathcal{R}\{A_{\mathrm{LF}}A_{\mathrm{HF}}^*\} e^{-\gamma|k|} \left(\sum_{n'=-N+1}^{N-1} c(n,n',k) e^{j2\pi 2\alpha n' k} \right) e^{j2\pi(f_{\mathrm{LF}}+2\alpha n+\beta)k} \\ &\quad + \frac{1}{2N-1} e^{-\gamma|k|} \left(\sum_{n'=-N+1}^{N-1} w(n+n'+k)w^*(n+n'-k) \right). \end{aligned} \tag{A.3}$$

Finally

$$\begin{aligned} r_x(n,k) &= |A_{\mathrm{LF}}|^2 e^{-\gamma|k|} e^{j2\pi f_{\mathrm{LF}}2k} + \frac{1}{2N-1} |A_{\mathrm{HF}}|^2 e^{-\gamma|k|} \frac{\sin(2\pi 2\alpha(2N-1)k)}{\sin(2\pi 2\alpha k)} e^{j2\pi f_{\mathrm{HF}}(n)2k} \\ &\quad + \frac{1}{2N-1} 2\mathcal{R}\{A_{\mathrm{LF}}A_{\mathrm{HF}}^*\} e^{-\gamma|k|} \left(\sum_{n'=-N+1}^{N-1} c(n,n',k) e^{j2\pi 2\alpha n' k} \right) \\ &\quad \times e^{j2\pi(f_{\mathrm{LF}}+f_{\mathrm{HF}}(n))k} \\ &\quad + r_w(n,k), \end{aligned} \tag{A.4}$$

where

$$r_w(n,k) = \frac{1}{2N-1} e^{-\gamma|k|} \left(\sum_{n'=-N+1}^{N-1} w(n+n'+k)w^*(n+n'-k) \right). \tag{A.5}$$

Appendix B.

Derivation of the constrained LS estimator of (18) using Lagrange multipliers. Taking the derivative of (18) with respect to $\mathbf{b}^*(n)$ and setting it equal to zero yields

$$\frac{\partial J_{c,n}}{\partial \mathbf{b}^*(n)} = \mathbf{R}_{\mathbf{x}}^H(n)\mathbf{r}_{\mathbf{x}}(n) + \mathbf{R}_{\mathbf{x}}^H(n)\mathbf{R}_{\mathbf{x}}(n)\mathbf{b}(n) + \frac{1}{2}\lambda \mathbf{z}_{\mathrm{HF}}^*(n) = 0. \tag{B.1}$$

The constrained LS estimator of $\mathbf{b}(n)$ is given by

$$\hat{\mathbf{b}}_{\mathbf{c}}(n) = \hat{\mathbf{b}}(n) - \frac{1}{2}\lambda \left(\mathbf{R}_{\mathbf{x}}^H(n)\mathbf{R}_{\mathbf{x}}(n) \right)^{-1} \mathbf{z}_{\mathrm{HF}}^*(n). \tag{B.2}$$

Substituting (B.2) in (17), the Lagrange multiplier λ can be found,

$$\lambda = 2[\hat{\mathbf{b}}^T(n)\mathbf{z}_{\mathrm{HF}}(n) + 1] \left(\mathbf{z}_{\mathrm{HF}}^H(n) \left[\left(\mathbf{R}_{\mathbf{x}}^H(n)\mathbf{R}_{\mathbf{x}}(n) \right)^{-1} \right]^T \mathbf{z}_{\mathrm{HF}}(n) \right)^{-1}, \tag{B.3}$$

and finally,

$$\begin{aligned} \hat{\mathbf{b}}_{\mathbf{c}}(n) &= \hat{\mathbf{b}}(n) - \left(\hat{\mathbf{b}}^T(n)\mathbf{z}_{\mathrm{HF}}(n) + 1 \right) \left(\mathbf{z}_{\mathrm{HF}}^H(n) \left[\left(\mathbf{R}_{\mathbf{x}}^H(n)\mathbf{R}_{\mathbf{x}}(n) \right)^{-1} \right]^T \mathbf{z}_{\mathrm{HF}}(n) \right)^{-1} \\ &\quad \times \left(\mathbf{R}_{\mathbf{x}}^H(n)\mathbf{R}_{\mathbf{x}}(n) \right)^{-1} \mathbf{z}_{\mathrm{HF}}^*(n). \end{aligned} \tag{B.4}$$

References

[1] The Task Force of ESC and NASPE, Heart rate variability. Standards of measurement, physiological interpretation, and clinical use, Eur. Heart J. 17 (1996) 354–381.
[2] A. Bianchi, L. Mainardi, E. Petrucci, M. Signorini, M. Mainardi, S. Cerutti, Time-variant power spectrum analysis for the detection of transient episodes in HRV signal, IEEE Trans. Biomed. Eng. 40 (2) (1993) 136–144.
[3] F. Lombardi, A. Malliani, M. Pagani, S. Cerutti, Heart rate variability and its sympatho-vagal modulation, Cardiovasc. Res. 32 (1996) 208–216.
[4] A. Aubert, B. Seps, F. Beckers, Heart rate variability in athletes, Sports Med. 33 (12) (2003) 889–919.
[5] R. Bailón, J. Mateo, S. Olmos, P. Serrano, J. García, A. del Río, I. Ferreira, P. Laguna, Coronary artery disease diagnosis based on exercise electrocardiogram indexes from repolarisation, depolarisation and heart rate variability, Med. Biol. Eng. & Comput. 41 (2003) 561–571.
[6] R. Hainsworth, The control and physiological importance of heart rate, in: M. Malik, A. Camm (Eds.), Heart Rate Variability, Futura Publishing Company, Inc, New York, 1995, pp. 3–19.
[7] F. Cottin, Y. Papelier, Regulation of cardiovascular system during dynamic exercise: integrative approach, Crit. Rev. Physical Rehab. Med. 14 (1) (2002) 53–81.
[8] L. Mainardi, On the quantification of heart rate variability spectral parameters using time–frequency and time-varying methods, Phil. Trans. R. Soc. A 367 (2009) 255–275.
[9] L. Keselbrener, S. Akselrod, Selective discrete Fourier transform algorithm for time–frequency analysis: method and application on simulated and cardiovascular signals, IEEE Trans. Biomed. Eng. 43 (8) (1996) 789–802.
[10] O. Meste, B. Khaddoumi, G. Blain, S. Bermon, Time-varying analysis methods and models for the respiratory and cardiac system coupling in graded exercise, IEEE Trans. Biomed. Eng. 52 (11) (2005) 1921–1930.
[11] K. Martinmäki, H. Rusko, S. Saalasti, J. Kettunen, Ability of short-time Fourier transform method to detect transient changes in vagal effects on hearts: a pharmacological blocking study, Am. J. Physiol. Heart Circ. Physiol. 290 (2006) H2582–H2589.
[12] D. Verlinde, F. Beckers, D. Ramaekers, A.E. Aubert, Wavelet decomposition analysis of heart rate variability in aerobic athletes, Auton. Neurosci. 90 (1–2) (2001) 138–141.
[13] E. Toledo, O. Gurevitz, H. Hod, M. Eldar, S. Akselrod, Wavelet analysis of instantaneous heart rate: a study of autonomic control during thrombolysis, Am. J. Physiol. Regul. Integr. Comp. Physiol. 284 (2003) R1079–R1091.
[14] Y. Goren, L. Davrath, I. Pinhas, E. Toledo, S. Akselrod, Individual time-dependent spectral boundaries for improved accuracy in time–frequency analysis of heart rate variability, IEEE Trans. Biomed. Eng. 53 (1) (2006) 35–42.
[15] P. Novak, V. Novak, Time/frequency mapping of the heart rate, blood pressure and respiratory signals, Med. Biol. Eng. & Comput. 31 (2) (1993) 103–110.
[16] S. Pola, A. Macerata, M. Emdin, C. Marchesi, Estimation of the power spectral density in non-stationary cardiovascular time series: assessing the role of the time–frequency representations (TFR), IEEE Trans. Biomed. Eng. 43 (1) (1996) 46–59.
[17] L. Mainardi, N. Montano, S. Cerutti, Automatic decomposition of Wigner distribution and its application to heart rate variability, Methods Inf. Med. 43 (2004) 17–21.
[18] A. Bianchi, L. Mainardi, C. Meloni, S. Chierchia, S. Cerutti, Continuous monitoring of the sympatho-vagal balance through spectral analysis. Recursive autoregressive techniques for tracking transient events in heart rate signals, IEEE Eng. Med. Biol. Mag. 16 (5) (1997) 64–73.
[19] M. Orini, R. Bailón, P. Laguna, L. Mainardi, Modeling and estimation of time-varying heart rate variability during stress test by parametric and non parametric analysis, in: Proceedings of Computers in Cardiology, Vol. 34, http://cinc.mit.edu, 2007, pp. 29–32.
[20] S. Akselrod, D. Gordon, F. Ubel, D. Shannon, A. Barger, R. Cohen, Power spectrum analysis of heart rate fluctuations: a quantitative probe of beat-to-beat cardiovascular control, Science 213 (1981) 220–222.

[21] B. Pomeranz, R. Macaulay, M. Caudill, Assessment of autonomic function in humans by heart rate spectral analysis, Am. J. Physiol. 248 (1985) H151–H153.
[22] P. Grossman, K. Wientjes, Respiratory sinus arrhythmia and parasympathetic cardiac control: some basic issues concerning quantification, applications and implications, in: P. Grossman, K. Jansenn, D. Waitl (Eds.), Cardiorespiratory and cardiosomatic psycophysiology, Plenum Press, NY, 1986, pp. 117–138.
[23] M. Pagani, D. Lucini, O. Rimoldi, R. Furlan, S. Piazza, L. Biancardi, Effects of physical and mental exercise on heart rate variability, in: M. Malik, A. Camm (Eds.), Heart Rate Variability, Futura Publishing Company, Inc, New York, 1995, pp. 245–266.
[24] L. Bernardi, F. Salvucci, R. Suardi, P. Solda, A. Calciati, S. Perlini, C. Falcone, L. Ricciardi, Evidence for an intrinsic mechanism regulating heart rate variability in the transplanted and the intact heart during submaximal dynamic exercise? Cardiovasc. Res. 24 (12) (1990) 969–981.
[25] G. Blain, O. Meste, S. Bermon, Influences of breathing patterns on respiratory sinus arrhythmia in humans during exercise, Am. J. Physiol. Heart Circ. Physiol. 288 (2005) H887–H895.
[26] R. Bailón, P. Laguna, L. Mainardi, L. Sörnmo, Analysis of heart rate variability using time-varying frequency bands based on respiratory frequency, in: Proc. 29th Int. Conf. IEEE Eng. Med. Biol. Soc., IEEE-EMBS Society, Lyon, 2007, pp. 6674–6677.
[27] R. Perini, C. Orizio, G. Baselli, The influence of exercise intensity on the power spectrum of heart rate variability, Eur. J. Appl. Physiol. 61 (1990) 143–148.
[28] Y. Yamamoto, R. Hughson, J. Peterson, Autonomic control of heart rate during exercise studied by heart rate variability spectral analysis, J. Appl. Physiol. 71 (3) (1991) 1136–1142.
[29] J. Warren, R. Jaffe, C. Wraa, C. Stebbins, Effect of autonomic blockade on power spectrum of heart rate variability during exercise, Am. J. Physiol. 273 (1997) R495–R502.
[30] O. Anosov, A. Patzak, Y. Kononovich, P. Persson, High-frequency oscillations of the heart rate during ramp load reflect the human anaerobic threshold, Eur. J. Appl. Physiol. 83 (4–5) (2000) 388–394.
[31] W. Martin, P. Flandrin, Wigner-Ville spectral analysis of nonstationary processes, IEEE Trans. Acoust. Speech Signal Proc. 33 (6) (1985) 1461–1470.
[32] T. Claasen, W. Mecklenbräuker, The Wigner distribution - A tool for time–frequency signal analysis. Part II: discrete-time signals, Philips J. Res. 35 (1980) 276–300.
[33] P. Flandrin, W. Martin, Pseudo-Wigner estimators for the analysis of non-stationary processes, in: Proc. IEEE Acoust. Speech Signal Proc. Spectrum Est. Workshop II, 1983, pp. 181–185.
[34] O. Meste, G. Blain, S. Bermon, Influence of the pedalling frequency on the heart rate variability, in: Proc. 29th Int. Conf. IEEE Eng. Med. Biol. Soc., IEEE-EMBS Society, Lyon, 2007, pp. 279–282.
[35] R. Kumaresan, D. Tufts, Estimating the parameters of exponentially damped sinusoids and pole-zero modeling in noise, IEEE Trans. Acoust. Speech Signal Proc. 30 (1982) 833–840.
[36] R. Kumaresan, On the zeros of the linear prediction-error filter for deterministic signals, IEEE Trans. Acoust. Speech Signal Proc. 31 (1983) 217–220.
[37] R. Bailón, L. Sörnmo, P. Laguna, A robust method for ECG-based estimation of the respiratory frequency during stress testing, IEEE Trans. Biomed. Eng. 53 (7) (2006) 1273–1285.
[38] G. Moody, R. Mark, Development and evaluation of a 2-lead ECG analysis program, in: Proc. Comput. Cardiol., vol. 9, IEEE Computer Society Press, 1982, pp. 39–44.
[39] J. Mateo, P. Laguna, Analysis of heart rate variability in the presence of ectopic beats using the heart timing signal, IEEE Trans. Biomed. Eng. 50 (2003) 334–343.
[40] F. Villa, P. Castiglioni, G. Merati, P. Mazzoleni, M. Di Rienzo, Effects of pedalling on the high frequency components of HRV during exercise, in: Proceedings of Computers in Cardiology, Vol. 35, http://cinc.mit.edu, 2008, pp. 37–40.
[41] R. Perini, N. Fisher, A. Veicsteinas, D.R. Pendergast, Aerobic training and cardiovascular responses at rest and during exercise in older mean and women, Med. Sci. Sports Exerc 34 (2002) 700–708.
[42] Y. Arai, J. Saul, P. Albrecht, L. Hartley, L. Lilly, R. Cohen, W. Colucci, Modulation of cardiac autonomic activity during and immediately after exercise, Am. J. Physiol. Heart Circ. Physiol. 256 (1989) H132–H141.
[43] F. Cottin, Y. Papelier, P. Escourrou, Effects of exercise load and breathing frequency on heart rate and blood pressure variability during dynamic exercise, Int. J. Sports Med. 20 (1999) 232–238.
[44] K. Keissar, L. Davrath, S. Akselrod, Time-frequency wavelet transform coherence of cardio-respiratory signals during exercise, in: Proceedings of Computers in Cardiology, Vol. 33, http://cinc.mit.edu, 2006, pp. 733–736.